Chapter 26
Grindability and Surface Integrity of Nickel-Based Cast Superalloy IN-738 by Vitrified Alumina Wheel

Srinivasa Rao Nandam, A. Venugopal Rao, Amol A. Gokhale and Suhas S. Joshi

Abstract IN-738 is a Ni-based superalloy widely used for manufacture of industrial gas turbine blades and vanes in vacuum investment cast and precipitation hardened condition. The castings so produced undergo certain machining operations to achieve fitment accuracies in the engine assemblies. However, these alloys are categorized as difficult-to-cut materials due to complex composition, the presence of hard refractory elements, high strength, and hot hardness. Precision grinding operations on these alloys are generally carried out by the special machineries to achieve higher grindability and better surface integrity. The surface integrity plays a vital role in the functional performance of turbomachinery components. In the present work, an experimental study has been carried on an IN-738 LC superalloy having polycrystalline grain structure by a conventional surface grinding process using a low-cost and higher performance vitrified alumina wheel. Grindability of the alloy in terms of grinding ratio, specific grinding energy and surface integrity aspects such as surface roughness, surface hardening and microstructural changes was evaluated. The grinding swarf was also analyzed to evaluate the deformation cum failure mechanisms involved during the grinding process.

Keywords Superalloys · Vitrified alumina wheel · Grindability · Surface integrity · Grinding swarf

26.1 Introduction

Precipitation hardened nickel-based superalloys are widely used in the manufacture of hot section components (gas turbine blades and vanes) of modern industrial power generation gas turbines and aerospace engines due to their excellent high-temperature creep–rupture strength and hot corrosion resistance [1]. IN-738 alloy is a vacuum

S. R. Nandam (✉) · A. V. Rao
Defence Metallurgical Research Laboratory, DRDO, Hyderabad 500058, India
e-mail: srinivas.nandam@gmail.com

A. A. Gokhale · S. S. Joshi
Department of Mechanical Engineering, IIT Bombay, Mumbai 400076, India

melted and cast alloy which exhibits superior tensile and elevated temperature stress rupture properties comparable to those of the widely used alloy IN-713C along with substantially better sulfidation resistance [2]. The microstructure of IN738 is highly complex. The main alloying elements chromium, cobalt, and the refractory elements such as molybdenum, tungsten, tantalum contribute to solid solution strengthening of the face-centered cubic gamma (γ) phase, i.e., the austenitic nickel matrix. The alloy is strengthened by precipitation hardening due to mainly Ni_3 (Al/Ti), a gamma prime phase (γ') and other phases such as MC and $M_{23}C_6$ carbides from tantalum- and chromium-based, respectively [3]. The rich amount of chromium also forms a protective layer of chromium oxide (Cr_2O_3) during service which enhances the corrosion resistance.

Machining operations are essential in precision components to achieve stringent dimensional and geometrical accuracies, and high surface finish. Cutting forces and heat are generated in metal cutting as a result of plastic deformation of the layer being machined [4]. The significantly higher cutting forces and heat generated during machining are due to the high shear strength, fracture strain, hot hardness, and low thermal conductivity of nickel-based superalloys. These conditions result in rapid tool wear and severely affect the dimensional accuracy and surface integrity of the machined surfaces. Many researchers found that the metallurgical characteristics of the Ni-based superalloys like high strength matrix, hard intermetallics, hard abrasive particles, and the high work hardening effect are the primary reasons for the poor machinability [5, 6]. Further, the machinability of cast nickel-based superalloys is worse when compared with wrought alloys due to the presence of more refractory elements and the non-uniform grain structure of the former material.

Grinding process is generally used for machining of hard and difficult-to-cut materials to obtain the required dimensional and geometrical accuracies. The grindability of any engineering material is described by the grinding forces, grinding temperature, specific grinding energy, and grinding ratio etc. [7]. The high temperatures at the grinding zone cause possible thermal damage to the workpiece during grinding with abrasive grinding wheels. Hence, more attention has been paid to improve surface quality of aerospace alloys by reducing excessive heat and cutting forces during the grinding process [8]. The most commonly adopted techniques for controlling the above for grinding of cast nickel-based super alloys is creep feed grinding technique [9, 10]. The large depth of cut, long arc of cut, and very slow workpiece speed (feed) are the prominent features of the creep feed grinding process. But the creep feed grinding process is found to be one of the highly expensive processes due to the requirement of heavy duty machine tools, specially designed grinding wheels and high pressure coolant system. Therefore, affordability by small- and medium-scale industries is a major concern.

The surface integrity (SI) of a machined component is the sum of all the elements that describe the conditions existing on or at the surface. The term was coined initially by Field and Kahles in the year 1964 [11]. The SI mainly consists of surface topography and surface metallurgy. The former describes the surface roughness or lay or texture of the outermost layer of the component's surface and the latter describes the nature of the altered layers below the surface with respect to the base

or matrix material. The usual SI problems that exist after machining heat resistant superalloys as reported in the literature are surface texturing, cavities, cracking, metallurgical transformation, plastic deformation, increased microhardness, increased surface roughness, formation of tensile residual stresses and heat affected zone, recast or redeposited material, change of physical properties, etc. SI of the component is of prime concern especially in aerospace applications as the failures are primarily caused due to fatigue, creep, and stress corrosion etc. [12–15].

The cause and effect of process parameters on SI in machining were shown in Fig. 26.1.

The published literature on grindability and surface integrity aspects of nickel-based cast superalloys is scarce in the open literature. To understanding the mechanisms involved in grinding of Ni-based cast superalloy and to evaluate the performance of widely used grinding wheels, an experimental study was undertaken in the present work. A polycrystalline cast IN-738 LC alloy was used for this purpose. Grinding experiments were conducted using a conventional surface grinding machine with a vitrified alumina wheel. The grindability and surface integrity aspects were evaluated systematically.
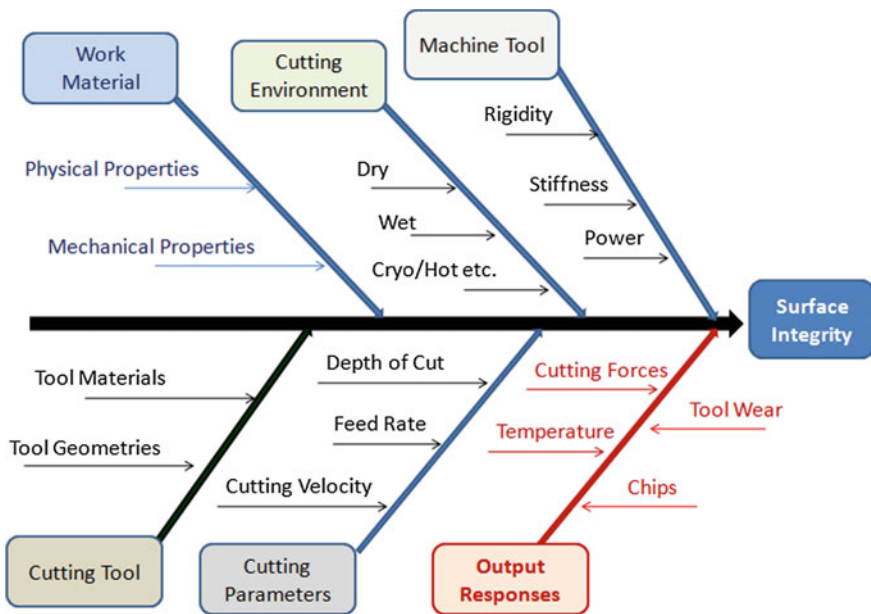

Fig. 26.1 Effect of machining parameters on SI

26.2   Experimental Setup

26.2.1   Work Material

A workpiece of 75 mm × 40 mm × 15 mm size was extracted by wire EDM process from a vacuum investment cast, polycrystalline structure component of IN-738 LC alloy. Rough EDM surfaces and heat affected zones of workpiece were removed by machining all the surfaces to a depth of 1 mm by milling process with multiple depths of cuts under flood coolant. The nominal chemical composition of the alloy by weight percentage is shown in Table 26.1 [16].

The physical and mechanical properties of the alloy published by INCO, alloy developers [17], are shown in Tables 26.2 and 26.3, respectively. The lower percentage of elongation indicates poor ductility (deformation) of the alloy.

26.2.2   Machine Tool

The grinding experiments were performed by a horizontal spindle type, precision conventional surface grinding machines of model PRAGA 452P from M/s HMT machine tools limited. The power rating of the main spindle of the machine was 1.5 kW, and the maximum running rotational speed was 2800 rpm.

26.2.3   Grinding Wheel

Vitrified aluminum oxide wheels are readily available in the open market with low cost and are regularly used for grinding high-strength structural steels. The grinding wheel used in these experiments was a conventional toolroom type, white color grinding wheel of specification A60K5V8 from M/s CUMI. The dimensions of the wheel were 200 mm of outer diameter and 20 mm of width with 31.75 mm of inner diameter for wheel mounting on the spindle. The specification of the grinding wheel is shown in Table 26.4.

26.2.4   Cutting Environment

The coolant used in the experiments was soluble cutting oil (neat oil), Servocut S product from M/s IOCL. The coolant was prepared with cutting oil of 5% concentration in water to form stable emulsion. Grinding experiments were conducted under flood coolant environment with flow rate of 50 l/min and 3 bar pressure.

Table 26.1 Chemical composition of IN-738 LC in weight percentage

C	Co	Cr	Mo	W	Ta	Nb	Al	Ti	Cu	Zr	Fe	Si	Ni
0.11	8.59	16.08	1.75	2.67	1.75	0.9	3.43	3.38	0.03	0.05	0.5	0.18	Bal

Table 26.2 Physical properties of the alloy

Property	Value at 20 °C	Value at 1093 °C
Density (kg/m^3)	8110	–
Dynamic modulus of elasticity (GPa)	201	201
Thermal conductivity (W/m/K)	11.8	27.3
Specific heat (J/Kg/°C)	418.4	711.3
Melting range (°C)	1230–1315	–
Coefficient of thermal expansion	6.45×10 E-6/°C	8.85×10 E-6
Poisson's ratio	0.28	0.30

Table 26.3 Mechanical properties of the alloy

Property	Value
0.2% yield strength	896 MPa
Tensile strength	1034 MPa
% Elongation	7
% Reduction of area	9
Impact properties at room temperature	76 J

Table 26.4 Specification of A60K5V8 grinding wheel [18]

Nomenclature	Description	Type
A	Abrasive	Aluminum oxide
60	Grit number	Medium
K	Grade (hardness)	Medium
5	Structure	Dense
V	Bond material	Vitrified
8	Abrasive	Aluminum oxide

26.2.5 Dynamometry

Various mechanisms such as rubbing, plowing, shearing, fracturing contribute to grinding forces during grinding process [19]. Piezoelectric-based precision cutting force dynamometer, model 9265B from M/s Kistler, Switzerland, was mounted on the magnetic table of surface grinding machine. A multicomponent (eight channels) charge amplifier model 5080A was used for amplifying analog signal of piezoelectric sensors (electrical charge). A data acquisition system, digital-to-analog converter (DAC) model 5697A was used to convert this amplified charge into analog data of cutting forces. A personal computer-based software Dynoware was used for analysis

Table 26.5 Grinding parameters

Parameter	Value
Length of stroke table	118 mm
Number of strokes per minute	40
Table traverse speed	4.7 m/min
Table cross-feed	0.7 mm/stroke
Table cross-speed	28 mm/min
Spindle rotational speed	2800 rpm
In-feed (depth of cut)	0.05 mm

of the cutting force data in terms of the maximum and minimum cutting forces in perpendicular *x*- and *z*-axes.

26.3 Experimentation

The wheel was trued and dressed by a single point diamond point dresser mounted on the table and positioned below the wheel. The angle of the dresser was 7.5° to the vertical plane, which was parallel to the front surface of the grinding wheel. The dressing operation was carried out with a depth of 0.05 mm under manual feed in two passes. The grinding parameters used during the experiments are shown in Table 26.5.

26.4 Results and Discussion

26.4.1 Grinding Swarf

The grinding swarf was collected from the surface table immediately after the grinding experiments. The fragmented particles of alumina and metallic chips of various configurations were observed under 50× magnification by a binocular optical digital microscope of model DM6000 M from M/s Leica, Germany. The fragmented particle of alumina is shown in Fig. 26.2a. The size of the majority of the particles was found to be 300–400 µm. Figure 26.2b shows a curved slice type chip from the work material of size around 800–900 µm. The signs of plastic deformation of the chips indicate ductile fracture from gamma phase matrix. The curvature of the chip might be due to the restriction to the free flow of the chips by the abrasives or the bond material. Tso [20] has also observed similar slice type of chips when grinding Inconel 718 by CBN grinding wheel in surface grinding operation. Figure 26.2c shows irregular shaped fragments of chips of around 200 µm. These might be brittle
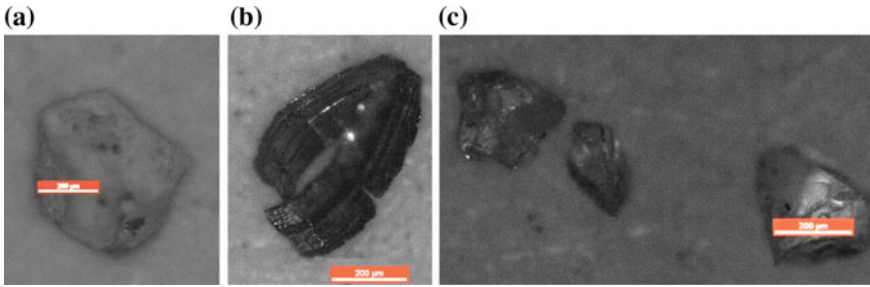
Fig. 26.2 a Fragments of alumina, **b** metallic chip, **c** fragments of intermetallic chips

fragments of intermetallic phase, gamma prime precipitates, which are found to be existed around 40% of volume fraction in the alloy.

26.4.2 Grindability

Material Removal Rate (MRR): The MRR was calculated based on weight loss method. The sample was weighed before and after grinding experiments by an electronic precision weight balances of 0.001 g least count. The readings recorded were 452.6 and 451.5 g, respectively. The calculated weight difference of 1.11 g indicates the material removal during the grinding process. The product of surface area of the work material and depth of cut gives the volume of material removed. The calculated volume of material removal was 150 mm^3. The corresponding weight of the material can be removed is 1.22 g. It was a bit higher than the actual value of 1.11 gm. The actual depth of cut calculated from the experimental material removal was 0.045 mm, which is very near the set value of 0.05 mm. The deviation of depth of cut value of 0.005 mm (10%) might be due to deflection of machine spindle due to thrust force from the work material and progressive wear out of the grinding wheel at higher values of in-feed.

Grinding Forces: The tangential cutting force (Fx) along the grinding direction and normal cutting force (Fz) parallel to depth of cut during the grinding process were measured. The maximum tangential cutting force was 26.98 N, and the maximum normal cutting force was 51.27 N. The signatures of cutting forces recorded are shown in Fig. 26.3a, b. It is observed that the cutting forces increase during the grinding process. Similar trend was observed by many researchers during machining of superalloys due to work hardening effect. But, in the present study, the calculated hardness values at machined surface shown in Table 26.6 indicate a lower surface hardness than bulk material. The increase in cutting forces might be due to loading and rubbing of the grinding wheel while progressing of grinding process.

Grinding Ratio: Grinding ratio is defined as the ratio of the volume of work material removed and the volume of wear of the grinding wheel. The initial and
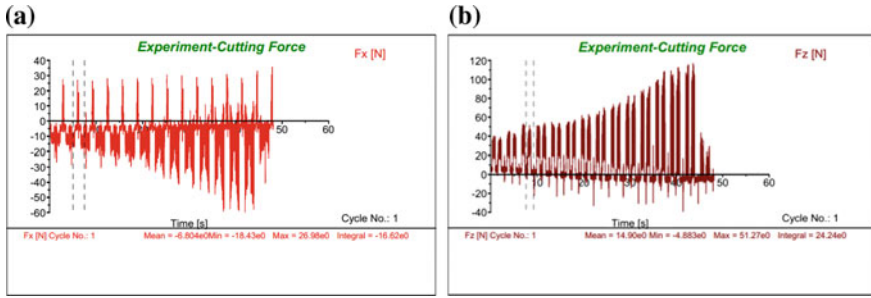
(a)   **(b)**

Fig. 26.3 a Tangential cutting force (Fx). **b** Normal cutting force (Fz)

Table 26.6 Readings of surface hardness of ground surface

Reading	1	2	3	Bulk
R1	344.0	347	349	359
R2	349.0	360	351	351
R3	351.0	364	352	353
Avg.	348.0	357.0	350.7	354.3

the final diameters of the grinding wheel after dressing, as measured by a precision micrometer of 0.01 mm least count, were 199.95 and 199.30 mm, respectively. The calculated number of strokes required to machine the width of workpiece of 40 mm under a cross-feed of 0.7 mm per stroke was 58 strokes. The calculated time to complete the 58 strokes with table speed of 40 strokes per minute was 1.45 min. The calculated volume of wear of the grinding wheel was 4391 mm^3. The volume rate of wear of grinding wheel per minute was 3028 mm^3. The calculated value of the volume of material removal of work material per minute was 9440 mm^3. Therefore, the calculated grinding ratio was 3.2. The general surface grinding process indicates the value of 50 for easy to grind materials and three for difficult to grind materials [7] due to reasonably higher wear of grinding wheel and lower material removal of work material.

Specific Grinding Energy: The specific grinding energy (J/mm^3) is defined as the energy required for removal of unit volume of material from the work material. The multiple of cutting force and the spindle speed gives the power consumption of the machine tool during grinding process. The calculated spindle speed was 29.2 m/s for 199.3 mm diameter grinding wheel at wheel rotational speed of 2800 revolutions per minute. The calculated power consumption was 1497 W for the maximum normal cutting force of 51.27 N. This value was very near (99.8%) to the value of spindle power of the machine tool (1500 W). The calculated specific grinding energy was 19 J/mm^3. Similar value of 27 J/mm^3 was observed by Ravuri et al. [21] in surface grinding of Inconel 718 by a standard resin bonded alumina wheel (A80K6B) of higher width (25 mm).

26.4.3   Surface Integrity Aspects

The Surface Roughness: The surface roughness was measured by a 2 μm coni-sphere-shaped diamond stylus with touch probe roughness measurement instrument of Form Talysurf Intra model from M/s Taylor Hobson, UK. The measurement was carried out on the ground surface at three different locations along and across the length of the workpiece. The sampling length selected was 10 mm, and the cutoff length selected was 0.8 mm with a spacing of 0.5 mm as per ISO 3274 standard. The average value of the surface roughness (Ra) achieved was 0.1 μm along the length and 0.6 μm across the length of workpiece. The achieved surface roughness value was much below the value of 1.0 μm of investigations by Ding et al. [9] and Caggiano and Teti [22] with CBN grinding wheels. The improvement of surface roughness might be due to the rubbing and polishing effect of the alumina abrasives.

Surface Hardness: The hardness values were measured on the machined surface at three locations with 20 kg load at three different positions by a standard Vickers hardness measuring machine, model VRS 270 from M/s Affri, Italy, with a diamond pyramid indenter. The average value was found to be 351.9 VHN. This value was very near to the surface hardness of bulk material of 354.3 VHN. The measured hardness values of machined surface and bulk surface were shown in Table 26.6. Many of the researchers have observed the increase of surface hardness on the machined surface due to surface hardening or work hardening effect during machining process [23, 24]. But few researchers have observed decrease in surface microhardness on nickel-based superalloy due to the effect of thermal softening [25, 26]. The minor decrease of surface hardness (around 1–2%) in this study might be either due to above thermal softening effect or microstructural modification of surface of work material.

Microstructural Evaluation: Two samples of 20 mm × 20 mm size were cut by WEDM process perpendicular to the machined surface from the work component. These samples were mounted in Bakelite mold under hot pressing, and care has been taken to orient machined surface as the top surface for one sample and un-ground surface as the top surface of the latter one. Metallography sample preparation was carried out by standard method using SiC bonded papers of 200–1200 grit size. These samples were cleaned by acetone and smooth cloth. Further polishing was done by lapping process with diamond paste of various sizes start from 9 to 1 μm. The cleaned sample surface was etched under standard Kalling's 2 reagent water-based solution by dip etching process. These samples were examined under optical microscope under various magnifications are shown in Fig. 26.4. Figure 26.4a, c, e are optical images of un-ground sample under 12.5×, 200× and 500× magni-fications, respectively, while Fig. 26.4b, d, and f are of the machined surfaces at comparable magnifications. It was observed from Fig. 26.4b that the dendrite struc-ture has certain modifications when compared with un-ground surface. Zhou [27] has observed surface deformation when IN-718 was turned under high-speed machining with SiC whisker reinforced alumina cutting tool. Zhang et al. [28] have observed recrystallized grains and formation of γ–γ′ eutectics when annealed and cellular recrystallised structure of a nickel-based cast superalloy heat treated below γ′ solvus
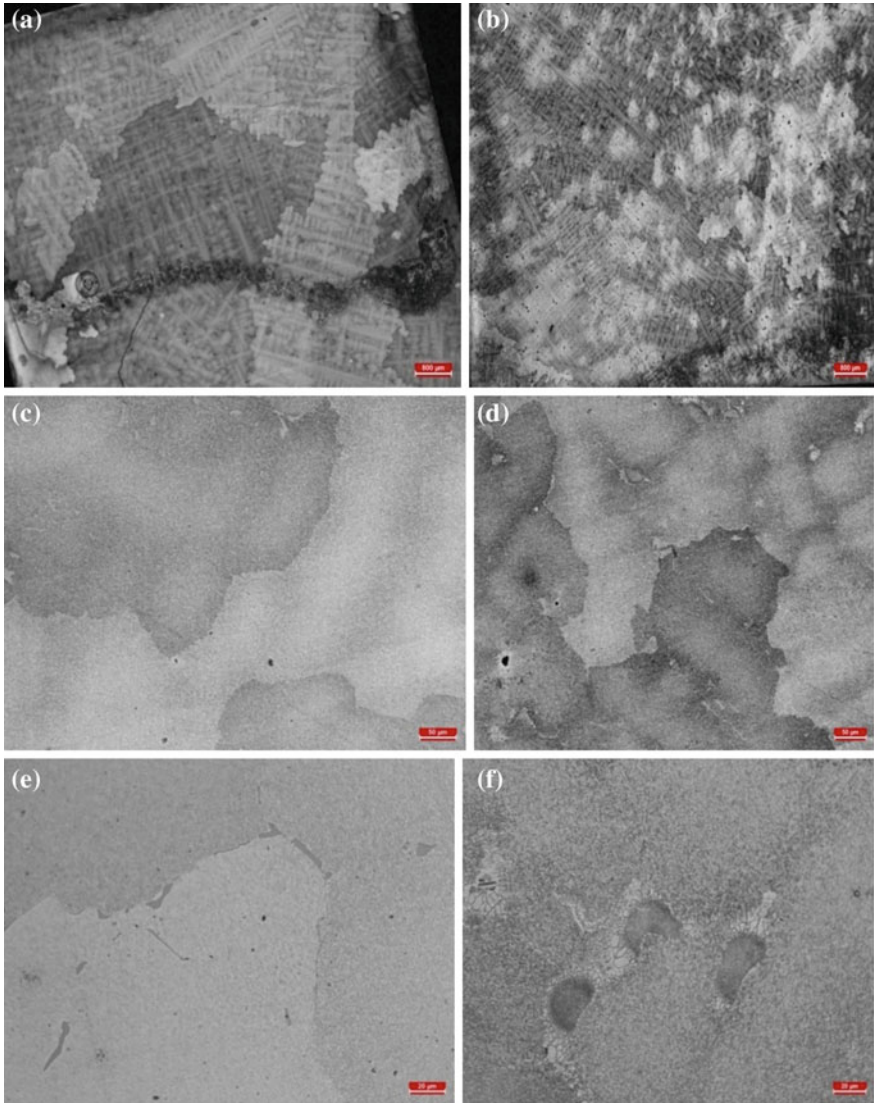
Fig. 26.4 **a** Un-ground surface at 12.5×, **b** ground surface at 12.5×, **c** un-ground surface at 200 ×, **d** ground surface at 200×, **e** un-ground surface at 500×, **f** ground surface at 500×

temperatures. The γ' solvus temperatures for IN-738 alloy found to be in the range of 1160–1175 °C. The similar re-crystallizations were also observed (Fig. 26.4d, f) in the present study. This was due to the thermomechanical effect on the machined surface by grinding process at much lower γ' solvus temperatures of the alloy.

26.5 Conclusions

The specific grinding energy of IN-738 alloy evaluated by a conventional surface grinding process with a toolroom purpose vitrified alumina grinding wheel was 19 J/mm^3. The overall grinding efficiency achieved was 99.8%. The lower value of grinding ratio 3.2 was due to reasonably higher wear of alumina grinding wheel. The wear of abrasives also attributed for formation of new and sharp cutting edges for successive grinding operations. The dimensional accuracy of 0.005 mm was achieved on the machined surface. The average surface roughness value of Ra achieved on the machined surface is 0.1 μm along the length. The rubbing and polishing actions of grinding wheel were predominant to achieve higher surface finish. The ductile and brittle fractures have found to be existed in the work material. The nickel phase matrix has contributed for ductile fracture, and where intermetallic precipitates of the gamma prime phase have contributed for brittle fracture during grinding process. Though any notable increase in surface hardness was not observed on the machined surface, minor microstructural changes were observed. As a consequence, the vitrified alumina grinding wheels can be proficiently used for simpler geometries to save machining time of costlier creep feed grinding process in the manufacture of turbomachinery components.

References

1. Pospisilova, S., Podrabsky, T., Stransky, K., Dobrovska, J.: Heterogenity of Inconel 713 LC and Inconel 738 LC, TMT 2006, pp 249–252. Spain (2006)
2. Egbewnde, A.T., Buckson, R.A., Ojo, O.A.: Analysis of laser beam weldability of Inconel 738 superalloy. Mater. Charact. **61**, 569–574 (2010)
3. Geddes, B., Leon, H., Huang, X.: Superalloys, Alloying and Performance. ASM International, Ohio (2010)
4. Shaw, M.C.: Metal Cutting Principles. Oxford Science Publications, USA (1984)
5. Komanduri, R., Schroeder, T.A.: On shear instability in machining a nickel iron base superalloy. Trans. ASME, J. Eng. Ind. **108**, 93–100 (1986)
6. Arunachalam, R., Mannan, M.A.: Machinability of nickle-based high temperature alloys. J. Mach. Sci. Technol. **4**(1), 127–168 (2000)

7. Boothroyd, G., Knight, W.A.: Fundamentals of Machining and Machine Tools, 3rd edn. CRC Press, Taylor & Francis Group, England (2013)
8. Aspinwall, D.K., Soo, S.L., Curtis, D.T., Mantle, A.L.: Profiled superabrasive grinding wheels for the machining of a nickel-based superalloy. Ann. CIRP **56/1**, 335–338 (2007)
9. Ding, W., Xu, J., Chen, Z., Su, H., Fu, Y.: Grindability and surface integrity of cast nickel-based superalloy in creep feed grinding with CBN abrasive wheels. Chin. J. Aeronaut. **23**, 501–510 (2010)
10. Cameron, A., Bauer, R., Warkentin, A.: An investigation of the effects of wheel-cleaning parameters in creep-feed grinding. Int. J. Mach. Tools Manuf. **50**, 126–130 (2010)
11. Guy, B., Tishler, N.: Introduction to Surface Integrity, Pamplet 1, TM70-974, GE, Aircraft Engine Group, Cincinnati, USA (1970)
12. Arunachalam, R.M., Mannan, M.A., Spowage, C.: Surface integrity when machining age hardened IN 718 with coated cutting tools. Int. J. Mach. Tools Manuf. 1481–1491 (2004)
13. Saoubi, R.M., Outeiro, J.C., Chandrasekaran, H., Dillon Jr., O.W., Jawahir, I.S.: A review of surface integrity in machining and its impact on functional performance and life of machined products. Int. J. Sustain. Manuf. **1**(1/2), 203–236 (2008)
14. Pawade, R.S., Suhas, S., Joshi, P.K.: Brahmankar, Effect of machining parameters and cutting edge geometry on surface integrity of high-speed turned IN718. Int. J. Mach. Tools Manuf. **48**, 15–28 (2008)
15. Thakur, A., Gangopadhyay, S.: State-of-the-art in surface integrity in machining of nickel-based superalloys. Int. J. Mach. Tools Manuf. **100**, 25–54 (2016)
16. Vadayar, S., Rani, S.D.: Hot corrosion behaviour of nickel based superalloy. Int. J. Appl. Res. Mech. Eng. (IJARME) **3**(1), 2231–5950 (2013)
17. Alloy IN-738 Technical Data, pp. 1–11. The International Nickel Company, Inc., New York
18. Technical Catalogue of Vitrified Tool Room Grinding Wheels, Carborundum Universal Limited, Chennai. https://www.cumi-murugappa.com/abrasives
19. Sinha, M.K., Ghosh, S., Paruchuri, V.R.: Modelling of specific grinding energy for IN718 superalloy. Proc. IMechE Part B: J. Eng. Manuf. 1–18 (2017)
20. Tso, P.-L.: An investigation of chip types in grinding. J. Mater. Process. Technol. **53**, 521–532 (1995)
21. Ravuri, B.P., Goriparthi, B.K., Revuru, R.S., Anne, V.G.: Investigations on grinding of IN718 using newly developed graphene nano platelets impregnated grinding wheels, pp. 381-1–381-6. AIMTDR 2014, IIT Guwahati
22. Caggiano, A., Teti, R.: CBN grinding performance improvement in aircraft engine components manufacture. Procedia CIRP **9**, 109–114 (2013)
23. Sharman, A.R.C., Hughes, J.I., Ridgway, K.: Workpiece surface integrity and tool life issues when turning Inconel 718™ nickel based superalloy. Mach. Sci. Technol. **8**(3), 399–414 (2004)
24. Devillez, A., Lecoz, G., Dominiak, S., Dudzinski, D.: Dry machining of IN718 work piece surface integrity. J. Mater. Process. Technol. 1590–1598 (2011)
25. Yao, C.F., Jin, Q.C., Huang, X.C., Wu, D.X., Ren, J.X., Zhang, D.H.: Research on surface integrity of grinding Inconel718. Int. J. Adv. Manuf. Technol. **65**, 1019–1030 (2013)
26. Gupta, U., Hithesh, K., Nandam S.R., Appa Rao, G.: Performance evaluation of coated carbide tools in high speed turning of advanced P/M nickel based superalloy. J. Mater. Sci. Surf. Eng. **5**(6), 661–665 (2017)
27. Zhou, J.: Identification of subsurface deformation in machining of IN718. Appl. Mech. Mater. **117–119**, 1681–1688 (2012)
28. Zhang, B., Cao, X., Liu, D., Liu, X.: Surface recrystallization of single crystal nickel-based superalloy. Trans. Nonferrous Met. Soc. China **23**, 1286–1292 (2013)